Spherical Indentation Behavior of Asphalt Mixtures

E. A. Ossa[1] and A. C. Collop[2]

Abstract: The spherical indentation response of a dense bitumen macadam asphalt mixture with two different volume fractions of bitumen binder is investigated both experimentally and via an analytical model. The model for the indentation of bitumen developed by Ossa et al. in 2005, was used to study the spherical indentation behavior of the mixtures with good agreement when compared to experimental results. An extensive experimental study of the monotonic and recovery spherical indentation behavior is reported for a range of temperatures. In line with the predictions of the model, the monotonic indentation response of the mixtures exhibits a power-law dependence on the indentation force. The model is also successful in capturing the indentation recovery behavior of the mixtures. A comparison of the material parameters obtained from uniaxial compression and indentation tests showed that indentation tests can be used in an easy and reliable way to obtain the fundamental asphalt parameters. Further, parameters found from indentation tests implicitly account for the confining conditions generated by the aggregate particles below the indenter.

DOI: 10.1061/(ASCE)0899-1561(2007)19:9(753)

CE Database subject headings: Asphalt mixes; Deformation; Creep; Constitutive models; Nondestructive tests.

Introduction

One of the most common forms of surface failure in flexible pavements is permanent deformation or rutting. Rutting is strongly influenced by the constitutive behavior of the bituminous mixtures (asphalts) used in the upper layers. It is then necessary to understand the constitutive behavior of these mixtures in order to understand, predict, and prevent pavement rutting.

Over the years a number of different approaches have been used for the prediction of permanent deformation in asphalt mixtures. These approaches include:

1. The nonlinear correspondence principle (Schapery 1984): e.g., Lee and Kim (1998) and Zhao and Kim (2003);
2. Soil mechanics based theories: e.g., Nijboer (1948), Ramsamooj et al. (1998), and Deshpande and Cebon (1999);
3. Viscoelastic or viscoplastic models: e.g., Lytton et al. (1993), Long (2001), Huang et al. (2002), Collop et al. (2003), Huang et al. (2004), and Abbas et al. (2004); and
4. Particle-contact based models: e.g., Chang and Meegoda (1993), Cheung et al. (1999), and Zhu and Nodes (2000).

However, these constitutive models often do not incorporate the dilatancy effects observed in experiments, or only apply to steady-state deformation behavior. Additionally, some of these models require many parameters or calibration tests, which make them difficult and cumbersome to use.

Recently, Ossa et al. (2004a) proposed a phenomenological model for asphalt that captured its response over a wide range of temperatures, stresses, and loading conditions. The model is simple and requires a minimum number of tests to calibrate all the model parameters under compressive conditions.

Indentation tests provide a cheap and easy method to measure the mechanical properties of materials. The standard indentation test on creeping solids involves either applying a constant load and measuring the indentation creep with time or by pressing the indenter into the material at a prescribed rate and measuring the load as a function of time. To interpret these results many researchers have developed models to relate the indentation pressure to the constitutive response of the materials. Notably, Tabor (1951) proposed empirical relations to correlate the indentation pressure for rate independent strain hardening solids to the uniaxial tensile response of the material, while Mulhearn and Tabor (1960) extended these empirical relations to power-law creeping materials. Using the similarity transformations for the indentation of metals developed by Hill et al. (1989), Bower et al. (1993) provided a rigorous theoretical basis for the empirical relations developed by Mulhearn and Tabor (1960) for rate dependent solids. Ossa et al. (2005) extended the model of Bower et al. (1993) to model the spherical indentation behavior of bitumen with good agreement with experimental results at various loading and temperature conditions.

Scope and Motivation of Study

The focus of this study is to investigate the monotonic and recovery spherical indentation response of asphalt with the aims of (1) validating the relevance of the indentation model for bitumen developed by Ossa et al. (2005) on asphalt mixtures; and (2) investigating the differences of the material properties found from compression and indentation experiments.

The outline of the paper is as follows. First, the constitutive model for asphalt of Ossa et al. (2004a) is briefly reviewed. Then, the indentation model for power-law creeping solids of Bower et al. (1993) is summarized and the indentation model for bitumen of Ossa et al. (2005) is briefly described. Later, an extensive experimental study of the monotonic and recovery spherical inden-

[1]Associate Professor, Production Engineering Dept., EAFIT Univ.
[2]Director, Nottingham Centre for Pavement Engineering, Univ. of Nottingham, University Park, Nottingham NG7 2RD, U.K.

Note. Associate Editor: Louay N. Mohammad. Discussion open until February 1, 2008. Separate discussions must be submitted for individual papers. To extend the closing date by one month, a written request must be filed with the ASCE Managing Editor. The manuscript for this paper was submitted for review and possible publication on November 29, 2005; approved on June 5, 2006. This paper is part of the ***Journal of Materials in Civil Engineering***, Vol. 19, No. 9, September 1, 2007. ©ASCE, ISSN 0899-1561/2007/9-753–761/$25.00.

tation behavior of two different asphalt mixtures is reported, and the predictions of the model compared with experimental measurements. Finally, the differences between the results found from indentation and compression tests will be discussed.

Deformation Behavior of Asphalt Mixtures

From a series of uniaxial experiments Deshpande and Cebon (2000) developed a relationship to characterize the steady-state deformation behavior of idealized asphalt mixtures over a wide range of temperatures, stresses, and strain rates. For temperatures well above the glass transition temperature T_g ($T \gg T_g$) of the bitumen, they showed that the transition from a linear viscous response at low stresses to nonlinear viscous behavior at high stresses is captured by the modified Cross model (Cross 1965; Cheung and Cebon 1997). This model relates the steady-state stress σ_{ss} and the steady-state strain rate $\dot{\epsilon}_{ss}$ through the relation

$$\frac{\sigma_{ss}}{\dot{\epsilon}_{ss}} = \frac{\sigma_0}{\dot{\epsilon}_0}\left(\frac{1}{1+\left(\frac{\dot{\epsilon}_{ss}}{\dot{\epsilon}_0}\right)^m}\right) \tag{1}$$

where σ_0 and $\dot{\epsilon}_0$=reference stress and strain rate, respectively; and the power-law parameter m governs the behavior of the asphalt in the nonlinear regime. The temperature behavior is controlled by "free volume" through the WLF relation

$$\dot{\epsilon}_0 = \dot{\epsilon}_{oc}\exp\left(\frac{2.303c_1^s(T-T_s)}{c_2^s(T-T_s)}\right) \tag{2}$$

where $\dot{\epsilon}_{oc}$=reference strain rate; T_s=reference temperature; and c_1^s and c_2^s="universal" constants equal to 8.86 and 101.6, respectively. Note that for high strain rates, $\dot{\epsilon}_{ss} \gg \dot{\epsilon}_0$, which corresponds to most practical operating conditions, the modified Cross model Eq. (1) reduces to a power-law creep relationship

$$\frac{\dot{\epsilon}_{ss}}{\dot{\epsilon}_0} = \left(\frac{\sigma_{ss}}{\sigma_0}\right)^n \tag{3}$$

where $n=1/(1-m)$.

Ossa et al. (2004b) performed an extensive experimental investigation of the deformation behavior of asphalt mixtures over a wide range of temperatures, strain rates, and stresses under monotonic, continuous cyclic, and cyclic pulse loadings. Based on these experimental observations, they wrote the total strain rate $\dot{\epsilon}$ as the sum of the rate independent elastic strain rate $\dot{\epsilon}^{el}=\dot{\sigma}/E$, the viscous strain rate $\dot{\epsilon}^v$, which is active during loading (i.e., when the applied stress $\sigma \neq 0$), and the recovery strain rate $\dot{\epsilon}^r$, which is only active when the stress $\sigma=0$. Thus, for an arbitrary loading history, the total strain rate is given by

$$\dot{\epsilon} = \dot{\epsilon}^{el} + \dot{\epsilon}^v + \dot{\epsilon}^r \tag{4}$$

In the high loading rate limit, the viscous strain rate is written in terms of the power-law relation

$$\dot{\epsilon}^v = \frac{\dot{\epsilon}^{pl}}{\beta} = \dot{\epsilon}_0(\epsilon)\left(\frac{\sigma}{\sigma_0}\right)^n \tag{5}$$

where

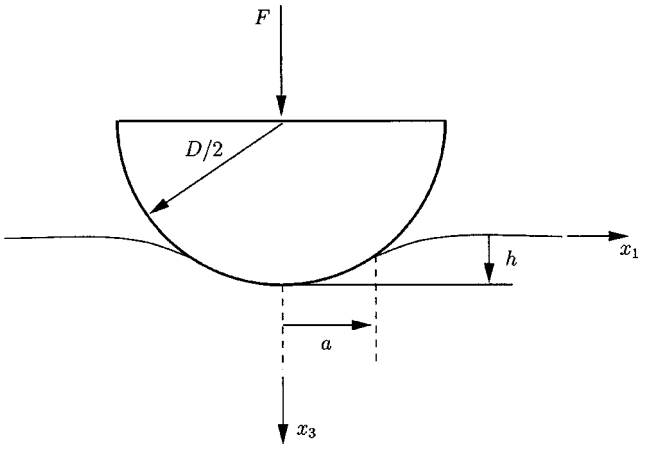

Fig. 1. Spherical indentation of half space. Notation and sign convention are shown.

$$\dot{\epsilon}_0(\epsilon) = \dot{\epsilon}_{oc}(\epsilon)\exp\left(\frac{2.303c_1^s(T-T_s)}{c_2^s(T-T_s)}\right) \tag{6}$$

and $\dot{\epsilon}^{pl}$=irrecoverable (or plastic) fraction of the viscous strain rate; while β="plasticity constant" for the particular mixture. The recovery rate is specified as

$$\dot{\epsilon}^r = -\,\text{sign}(\epsilon)[1-\text{sign}(|\sigma|)]\dot{\epsilon}_u(\hat{\epsilon}^r) \tag{7}$$

where sign(0) is defined to be zero

$$\hat{\epsilon}^r = \left(\frac{\epsilon}{\epsilon^{pl}}-1\right)\frac{\beta}{1-\beta} \tag{8}$$

and

$$\dot{\epsilon}_u(\hat{\epsilon}^r) = \dot{\epsilon}_{uc}(\hat{\epsilon}^r)\exp\left(\frac{2.303c_1^s(T-T_s)}{c_2^s(T-T_s)}\right) \tag{9}$$

Note that $\dot{\epsilon}_{oc}(\epsilon)$ and $\dot{\epsilon}_{uc}(\hat{\epsilon}^r)$=loading and recovery calibration functions. These are unique functions of the strains ϵ and $\hat{\epsilon}^r$ and govern the strain hardening/softening behavior of the asphalt mixture. Eqs. (4)–(9) can be integrated with respect to time to obtain the strain resulting from any applied stress history.

The constitutive model detailed above was developed for uniaxial loading. After an extensive triaxial testing study, Ossa et al. (2004a, 2006) generalized this model to multiaxial loading by noting that the response of asphalt mixtures is dependent on the mean or hydrostatic stress. For a complete discussion of the three-dimensional constitutive behavior of asphalt mixtures the reader is referred to the works of Deshpande and Cebon (1999), Collop and Khanzada (2001), and Ossa et al. (2004a, 2006).

Indentation Behavior of Creeping Solids

Consider a half-space, occupying the region $x_3 \geq 0$ and loaded by a frictionless spherical rigid indenter of diameter D, as sketched in Fig. 1. The material in the half-space is assumed to deform according to a power-law creep law of the form

$$\frac{\dot{\epsilon}_{ij}}{\dot{\epsilon}_0} = \frac{3}{2}\left(\frac{\sigma_e}{\sigma_0}\right)^{n-1}\frac{\sigma'_{ij}}{\sigma_0} \tag{10}$$

where σ_0, $\dot{\epsilon}_0$, and n=material constants and the prime denoting deviatoric quantities.

J. Mater. Civ. Eng., 2007, 19(9): 753-761

Table 1. Indentation Model Parameters α and c as Function of Power-Law Exponent n [Adapted from Bower et al. (1993)]

n	α	c
1.00	0.849	0.707
1.11	1.085	0.747
1.25	1.332	0.788
1.43	1.602	0.831
1.66	1.886	0.875
2.00	2.176	0.920
2.50	2.465	0.966
3.33	2.734	1.013
5.00	2.973	1.065
10.00	3.110	1.128
100.00	3.051	1.201

Bower et al. (1993) solved the problem of the plane strain and axisymmetric indentation of a half-space comprising a power-law creeping solid Eq. (10), using the similarity transformations suggested by Hill et al. (1989). For indentation by a frictionless spherical indenter, the similarity solutions dictate that the contact radius a is related to the indentation depth h by

$$h = \frac{1}{c^2}\frac{a^2}{D} \tag{11}$$

where the constant c=unique function of the material constant n and may be thought of as the ratio of the true to nominal contact radius, where the nominal contact radius is $\sqrt{hD}$. Similarly, the applied load F is related to the indentation rate $\dot{h}$ via

$$\frac{F}{\pi a^2 \sigma_0} = \alpha\left(\frac{\dot{h}}{a\dot{\epsilon}_0}\right)^{1/n} = \alpha\left(\frac{2\dot{a}}{\dot{\epsilon}_0 c^2 D}\right)^{1/n} \tag{12}$$

where the constant α is again only a function of the power-law exponent n. Values of c and α for selected values of n were deduced by Bower et al. (1993) from a series of finite-element calculations and are listed in Table 1.

Eqs. (11) and (12) can be written in terms of *effective* stress and *effective* strain under the indenter. The effective stress σ^{eff} under the indenter is defined as

$$\sigma^{\text{eff}} = \frac{F}{\pi a^2} \tag{13}$$

while the effective strain rate and strain under the indenter are specified as

$$\dot{\epsilon}^{\text{eff}} = \frac{\dot{a}}{D} = \frac{c\dot{h}}{2\sqrt{hD}} \tag{14a}$$

and

$$\epsilon^{\text{eff}} = c\sqrt{\frac{h}{D}} \tag{14b}$$

respectively. Substituting these definitions in Eqs. (11) and (12) gives the empirical results of Mulhearn and Tabor (1960)

$$\sigma^{\text{eff}} = \alpha\sigma_0\left(\frac{2\dot{\epsilon}^{\text{eff}}}{c^2\dot{\epsilon}_0}\right)^{1/n} \tag{15}$$

for the pressure under an indenter in a power-law creeping solid.

Based on the concepts of *effective stress* σ^{eff} Eq. (13) and *effective strain* ϵ^{eff} Eq. (14*b*) under a spherical indenter, Ossa et al. (2005) extended the model of Bower et al. (1993) to predict the spherical indentation behavior of bitumen. In their model the indentation rate $\dot{h}$ is written as the sum of the elastic indentation rate $\dot{h}^{\text{el}}$, the viscous indentation rate $\dot{h}^{v}$, which is active during loading (indentation force $F \neq 0$), and the recovery rate $\dot{h}^{r}$, which is only active when $F=0$. For an arbitrary loading history, the strain rate $\dot{\epsilon}$ under the indenter is written as

$$\dot{\epsilon} = \dot{\epsilon}^{\text{el}} + \dot{\epsilon}^{v} + \dot{\epsilon}^{r} = \frac{c}{2\sqrt{hD}}\dot{h} = \frac{c}{2\sqrt{hD}}(\dot{h}^{\text{el}} + \dot{h}^{v} + \dot{h}^{r}) \tag{16}$$

where the elastic indentation rate is written as (Bower et al. 1993)

$$\dot{h}^{\text{el}} = \frac{2\dot{\epsilon}^{\text{el}}}{c(1)}\sqrt{hD} = \frac{\dot{F}}{\alpha(1)\pi a E} \tag{17}$$

The viscous indentation and strain rates are related to the indentation force via

$$\dot{h}^{v} = \frac{2\dot{\epsilon}^{v}}{c}\sqrt{hD} = \left(\frac{F}{\pi a^2 \sigma_0 \alpha}\right)^{n} a\dot{\epsilon}_0(\epsilon) \tag{18}$$

and $\dot{\epsilon}_0$ in Eq. (12) has been replaced by the strain dependent function $\dot{\epsilon}_0(\epsilon)$. The indentation recovery rate is given by

$$\dot{h}^{r} = \frac{2\dot{\epsilon}^{r}}{c}\sqrt{hD} = -\frac{2\sqrt{hD}}{c}[1 - \text{sign}(|F|)]\dot{\epsilon}_u(\hat{\epsilon}^{r}) \tag{19}$$

where $\hat{\epsilon}^{r}$ is specified by Eq. (8) with the irrecoverable strain rate $\dot{\epsilon}^{\text{pl}}$ related to the viscous strain rate via the *plasticity constant* β

$$\dot{\epsilon}^{\text{pl}} = \beta\dot{\epsilon}^{v} \tag{20}$$

Eqs. (16)–(19) completely specify the indentation behavior of bitumen: time integration of these equations provides the complete history of the indentation depth as a function of time for specified loading conditions.

Researchers like Deshpande and Cebon (1999), Collop and Khanzada (2001), and Ossa et al. (2004a) have found that the deformation behavior of asphalt mixtures is highly dependent on the deformation characteristics of the bitumen matrix, with the power law (n and σ_0) and temperature parameters remaining unchanged. However, unlike bitumen, the asphalt mixture response is governed by the mean stress σ_m, with the loading $\dot{\epsilon}_{oc}(\epsilon)$ and recovery $\dot{\epsilon}_{uc}(\hat{\epsilon}^{r})$ calibration functions depending on the strains ϵ and $\hat{\epsilon}^{r}$ and stress ratio η, with the equivalent stress ratio defined as

$$\eta = \frac{\sigma_m}{\sigma_e} \tag{21}$$

where σ_e=Von-Mises equivalent stress.

The relevance of the indentation model of Ossa et al. (2005) to predict the indentation behavior of asphalt mixtures and the effect of the confining conditions imposed by the aggregate on the indented half-space will be assessed in the following sections.

Experimental Investigation

Materials

A generic asphalt mixture corresponding to a 10 mm dense bitumen macadam (DBM), BS4987-1 (BSI 2003), was fabricated with two different fractions of bitumen binder, using (1) the amount specified in the standard (5.5% by mass); and (2) an in-

J. Mater. Civ. Eng., 2007, 19(9): 753-761

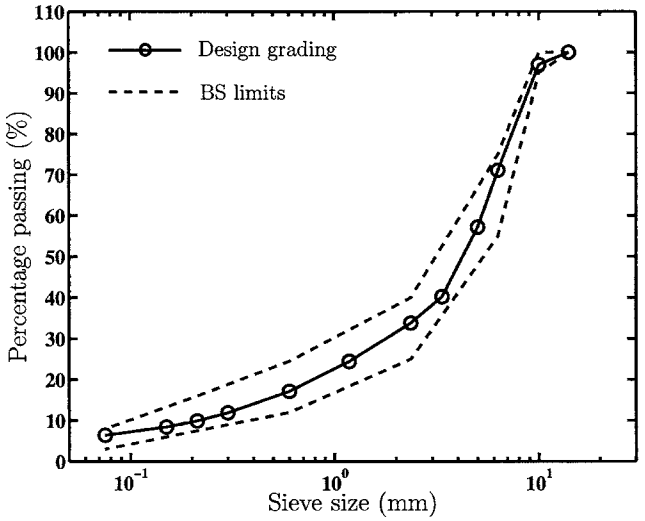

Fig. 2. Aggregate grading for 10 mm DBM mixtures

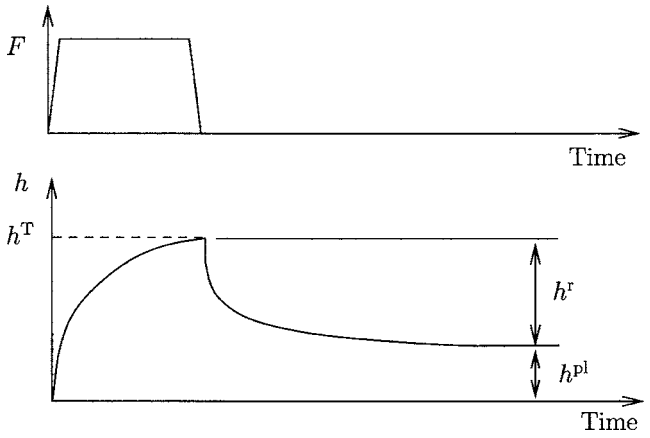

Fig. 3. Schematic showing load and indentation depth versus time histories in creep recovery indentation test

creased amount of binder (8.0% by mass), in order to assess the effect of an increase in bitumen content on the indentation behavior of the mixtures. A 70/100 penetration grade (pen) bitumen, with penetration and softening point values of 88 dmm and 45°C, respectively, was used for both mixtures. The two different DBM mixtures were made using angular granite aggregate with a maximum nominal size of 10 mm. Fig. 2 shows the design grading and the specification grading envelopes for the mixtures. The target air void content was chosen to be 4.0% for both mixtures, and the mixtures consisting of binder contents of 8.0 and 5.5% (by mass) are subsequently referred to as Mixtures A and B, respectively.

Specimen Preparation

Cylindrical specimens, 150 mm in diameter and 55 mm in height, were manufactured for the testing program. The diameter of the specimens was selected after studying various diameters, finding that diameters below 150 mm generate results with considerable variability, while with diameters of 150 mm and over the results were consistent and repeatable. The specimens were produced by cutting and trimming 150- mm-diameter Gyratory specimens compacted at a temperature between 150 and 156°C. The air void content was measured on the two halves after trimming to discard specimens with air void contents outside the 3–5% limits. The specimens were stored in a cold room at 5°C previous to testing.

Test Protocol

Spherical indentation tests on the specimens were performed in a hydraulic testing machine. The indentation load F was measured using a 10 kN load cell, while the load line displacement was employed to obtain the indentation depth h. The indenter diameter was selected keeping a ratio of indenter diameter to aggregate size of at least 10, in order to avoid contact with a single aggregate particle during the indentation process. The hardened steel spherical indenter of diameter 125 or 200 mm was lubricated with a thin layer of a mixture of soap and glycerine, allowing nearly *frictionless* indentation. This test condition was chosen in order to avoid the extra *confinement* conditions below the indenter caused by full friction. Typically indents to a depth $h \leqslant 5$ mm were performed with the indent affected zone much smaller than the cylindrical specimen dimensions. Thus, for all practical purposes, the tests may be regarded as indentation of a half-space of asphalt. The test temperature was controlled by performing the tests in an environmental chamber with a resolution of ±0.5°C fitted on the test machine. Prior to testing, all specimens were kept in the environmental chamber for about 2 h to allow them to attain the test temperature. Unless otherwise specified, a 200-mm-diameter spherical indenter was employed in this study. A few tests were conducted with a 125-mm-diameter indenter in order to confirm the predicted dependence of the indentation response on the indenter diameter. It should be noted that a number of spot repeat tests confirmed the reproducibility of the test results reported here. For the sake of brevity, these results are not presented.

Monotonic Indentation Tests

Constant indentation rate and constant load creep indentation tests were employed to characterize the monotonic indentation response of the asphalt mixtures. In the constant indentation-rate tests, a specified indentation rate $\dot{h}$ was applied by the indenter and the resulting load F and indentation depth h recorded. In the constant load creep indentation tests, a constant indentation load F was applied *instantaneously* (typically over 0.25 s) by the indenter and the indentation depth h recorded as a function of time t.

Creep Recovery Indentation Tests

The creep recovery indentation behavior of the mixtures was investigated by performing a series of single load/unload indentation tests as sketched in Fig. 3. A load F was applied rapidly by the indenter to the specimen and then held constant. The material was allowed to creep to a specified total indentation depth h^T. At this indentation depth, the load was released and the indentation depth monitored until the indentation rate $\dot{h} \approx 0$. The indentation depth at this point $h^{pl}=h^T-h^r$ is the irrecoverable indentation depth (Fig. 3). Such tests were repeated for a series of indentation depths h^T, loads F, and temperatures.

Experimental Results and Comparison with Model Predictions

The monotonic and recovery indentation experimental results are described in this section and the results compared with the pre-

J. Mater. Civ. Eng., 2007, 19(9): 753-761

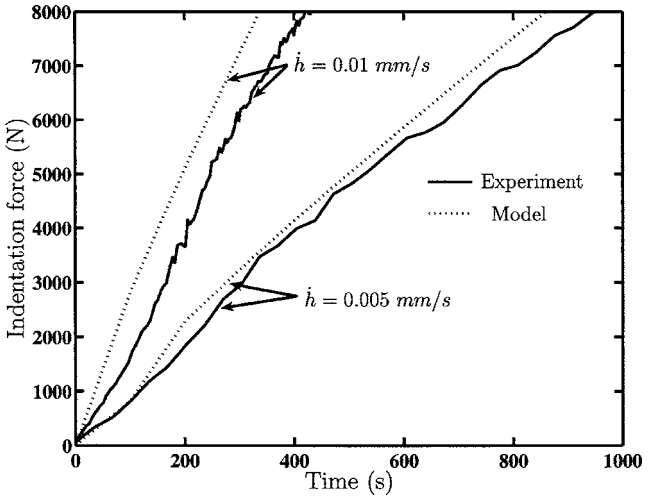

Fig. 4. Applied indentation force versus time for two selected values of applied indentation rate at 20°C with 200-mm-diameter spherical indenter on Mixture A. Experimental measurements and model predictions are included.

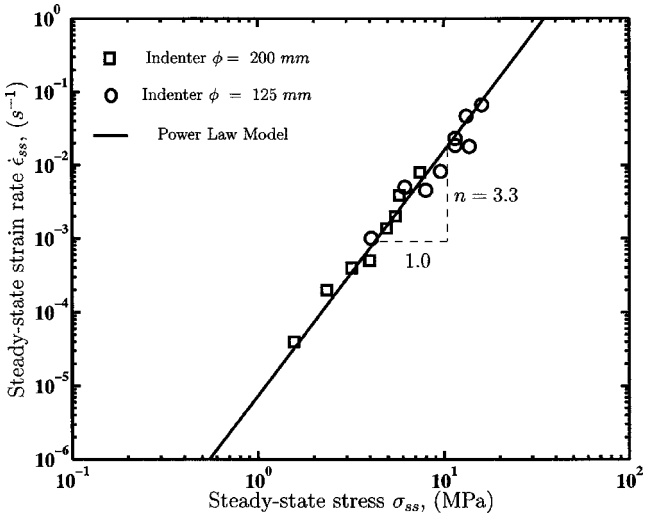

Fig. 6. Steady-state indentation behavior on Mixture A at 20°C. Experimental results obtained using two different indenter diameters are shown along power-law model, Eq. (3).

dictions of the indentation model described in "Discussion." Unless otherwise specified, the experiments reported were conducted at 20°C employing the 200-mm-diameter spherical indenter.

Monotonic Indentation Behavior

The measured indentation load F versus time t response of Mixture A for two selected values of the applied indentation rate $\dot{h}$=0.005 and 0.010 mm s^{-1} are plotted in Fig. 4. In both cases, the indentation load F increases monotonically with time and the slope of the F versus t curve increases with increasing indentation rate $\dot{h}$.

Results from two constant load creep indentation tests (F=4.0 and 9.0 kN) for Mixture A are plotted in Fig. 5. The indentation depth h versus time response comprises two regimes:

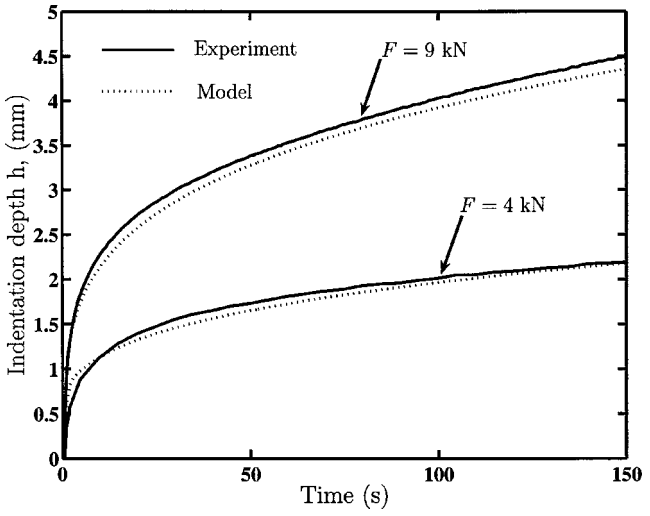

Fig. 5. Applied indentation depth versus time histories for two selected values of constant applied indentation force at 20°C with 200-mm-diameter spherical indenter on Mixture A. Experimental measurements and model predictions are included.

a primary creep regime where $\dot{h}$ decreases with time, followed by a secondary or steady-state creep regime, where $\dot{h}$ remains approximately constant. Increasing the indentation load F increases $\dot{h}$ over the full range of indentation depths considered here.

A plot of $\dot{\epsilon}_{ss}$ versus σ_{ss} corresponding to the steady-state region of the experimental results, using the definitions of *effective stress* σ^{eff} Eq. (13) and *effective strain rate* $\dot{\epsilon}^{eff}$ Eq. (14*a*) under the indenter, is shown in Fig. 6. The power-law model Eq. (3) with the constants listed in Table 2 was fitted to the steady-state experimental data of Mixture A in the same figure. Similar to the observations of Ossa et al. (2006) for similar mixtures in compression, the asphalt mixture exhibits nonlinear behavior with $\dot{\epsilon}_{ss} \propto \sigma_{ss}^{3.3}$ at the stresses and strain rates studied. Note that experimental data obtained with the two different indenter diameters (125 and 200 mm) are also included in Fig. 6, revealing that to within experimental error the results are independent of indenter diameter, in line with the definition of *effective* properties.

Predictions of the model are included in Figs. 4 and 5 showing good agreement with the experimental measurements. The loading strain dependent functions $\dot{\epsilon}_{oc}(\epsilon)$ used for modeling shown in Fig. 7 were extracted from selected monotonic experimental results using Eq. (18) along with the WLF relation (2).

Creep Recovery Indentation Behavior

Creep recovery indentation tests were performed at 20°C and the recovery behavior investigated for unloading from total effective

Table 2. Material Parameters for Asphalt Mixtures Studied

Parameter	Mixture A	Mixture B
n	3.3	4.0
σ_0 (MPa)	0.08	0.10
$\dot{\epsilon}_{oc}$ (s^{-1})	1.80×10^{-9}	4.66×10^{-11}
c	1.0113	1.0339
α	2.7243	2.8299
β	0.96	0.94
T_s (°C)	4	−5

J. Mater. Civ. Eng., 2007, 19(9): 753-761

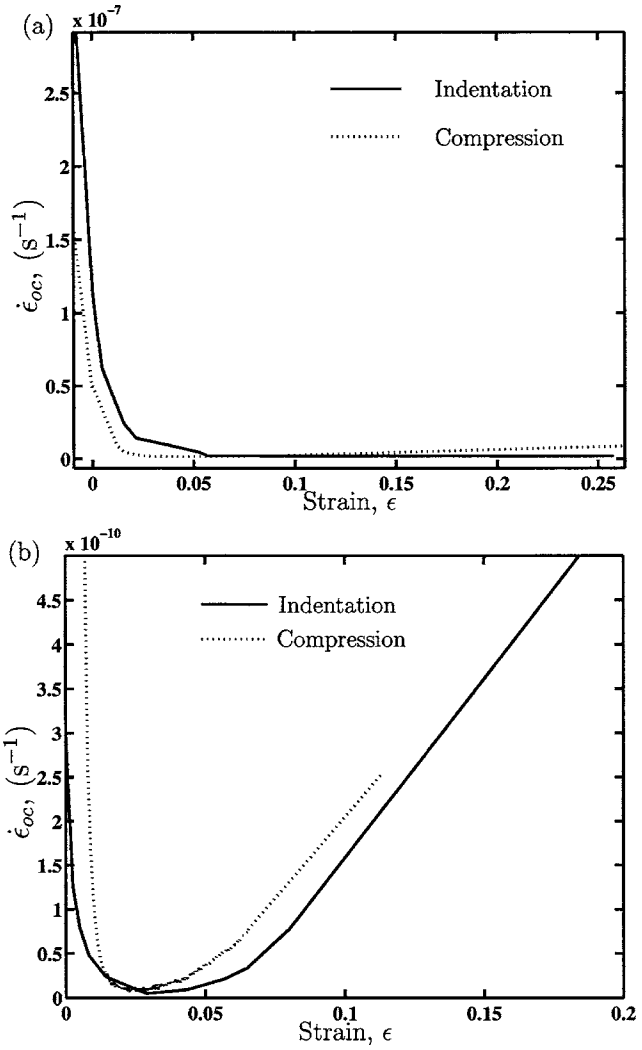

Fig. 7. Loading calibration curves obtained from compression and indentation tests: (a) for Mixture A; (b) for Mixture B

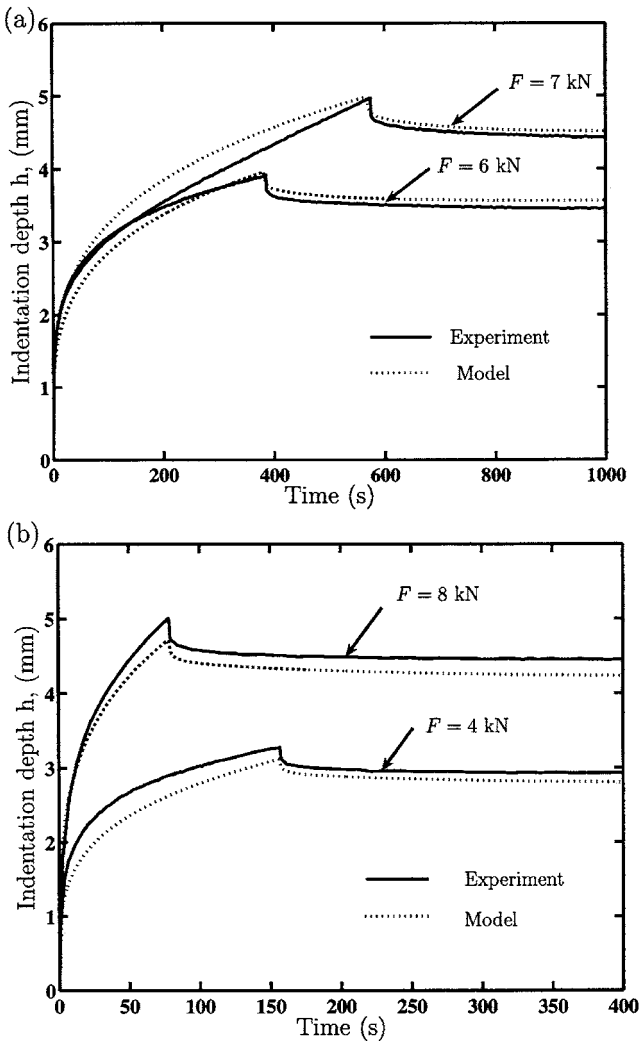

Fig. 8. Indentation creep recovery experimental measurements and model predictions at two selected values of total indentation depths h^T and indentation loads F at 20°C for Mixture A: (a) with spherical indenter of diameter ϕ=200 mm; (b) with spherical indenter of diameter ϕ=125 mm.

strains $\epsilon^T = c\sqrt{h^T/D}$ in the range $0.1 \leq \epsilon^T \leq 0.25$. Experiments were performed for different indentation loads for the two indenter diameters (125 and 200 mm). The creep recovery indentation response of Mixture A for different indentation loads and indenter diameters is shown in Fig. 8, where the indentation depth h is plotted as a function of time t. The irrecoverable indentation h^{pl} is lower for the larger h^T. This result is consistent with the observations of Ossa et al. (2004b) for asphalt in uniaxial compression, where it was shown that a larger initial compressive strain results in a lower irrecoverable strain.

Results from all the creep recovery indentation tests performed on Mixture A are summarized in Fig. 9 where the irrecoverable effective strain $\epsilon^{pl} = c\sqrt{h^{pl}/D}$ is plotted as a function of the total minus elastic effective strain $\epsilon^T - \epsilon^{el}$ prior to unloading. The figure reveals that, to within experimental error, the data are well represented by the line $\epsilon^{pl} = \beta(\epsilon^T - \epsilon^{el})$ with β ($0 \leq \beta \leq 1$) independent of the applied indentation load (effective stress), temperature, and indenter diameter. Moreover, the recovery experimental results from uniaxial compression tests on the same mixture are also plotted in Fig. 9, showing no variation on the value of $\beta \approx 0.96$ from indentation to compression conditions.

A comparison between model predictions and experimental measurements is included in Fig. 8 and indicates that the model captures both the loading and unloading indentation response of the mixture reasonably accurately. The recovery calibration functions $\dot{\epsilon}_{uc}(\dot{\epsilon}^r)$, used in modeling shown in Fig. 10, were extracted from selected experimental results using Eqs. (8) and (19) along with the WLF relation (2). Fig. 11 shows experiments and model predictions for creep recovery indentation tests performed at 15°C on Mixture A. The model reasonably predicts the recovery indentation behavior at this temperature, confirming the accuracy of the WLF relation (2) on predicting the temperature dependence of the material. It is worth noting here that the temperature parameter T_s used here was the same found by Ossa et al. (2006) for the same asphalt mixtures tested under compression at temperatures between 10 and 40°C. Therefore, it is expected that the indentation model would also be valid for temperatures between this range.

Results similar to those previously discussed for Mixture A were also obtained for Mixture B. Fig. 12 shows two selected creep recovery indentation test results performed on Mixture B at

J. Mater. Civ. Eng., 2007, 19(9): 753-761

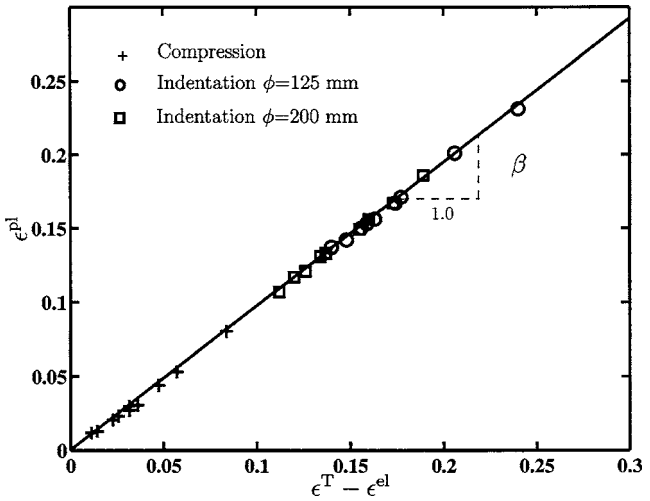

Fig. 9. Summary of indentation creep recovery experimental measurements on Mixture A. Experimental data for different levels of indentation force and indenter diameters show linear relationship between ϵ^{pl} and $\epsilon^{T}-\epsilon^{el}$ for two indenter diameters investigated. Also shown values found from compression tests.

20°C with the 200-mm-diameter indenter. As for Mixture A, the model predicts reasonably well the loading and unloading indentation behavior of the mixture.

Discussion

The spherical indentation response of two asphalt mixtures was investigated in this study and the model of Ossa et al. (2005) was used to analyze the monotonic and recovery indentation response of the material. Bower et al. (1993) presented a general analysis of the indentation behavior of creeping solids which is applicable to either plane strain or axisymmetric indenters of arbitrary geometries including conical and cylindrical indenters. An extension of the model of Ossa et al. (2005) presented here, could also be generalized to these cases on lines similar to that presented by Bower et al. (1993).

The two different amounts of bitumen (5.5 and 8.0% by mass) employed in the mixtures were found to have a significant effect on the deformation behavior. The higher binder content, Mixture A, was found to be "softer" than Mixture B, as confirmed by comparison of the values of the constants $\dot{\epsilon}_{oc}$ in Table 2. A higher value of $\dot{\epsilon}_{oc}$ reflects an increased deformation susceptibility of the mixture under particular loading conditions. Also note an increase on the power-law exponent n (see Table 2) on Mixture B. As bitumen films in Mixture B become thinner, the contact with hot aggregate particles during the mixing process leads to aging, which in turn hardens the bitumen and further increases the power-law exponent n of the mixture.

A comparison between the loading and recovery calibration curves obtained from indentation and compression tests is shown in Figs. 7 and 10, respectively, for the two mixtures studied. The general shape of the loading calibration curves $\dot{\epsilon}_{oc}(\epsilon)$ is the same, with an initial reduction in the strain rate, followed by a steady-state minimum, leading to an increase in strain rate representative of the tertiary creep region of behavior. However, note that the strain ϵ to reach a minimum value of $\dot{\epsilon}_{oc}$ is lower for the compressive results (for both mixtures). The aggregate below the indenter generates a state of *confinement* which allows for bigger

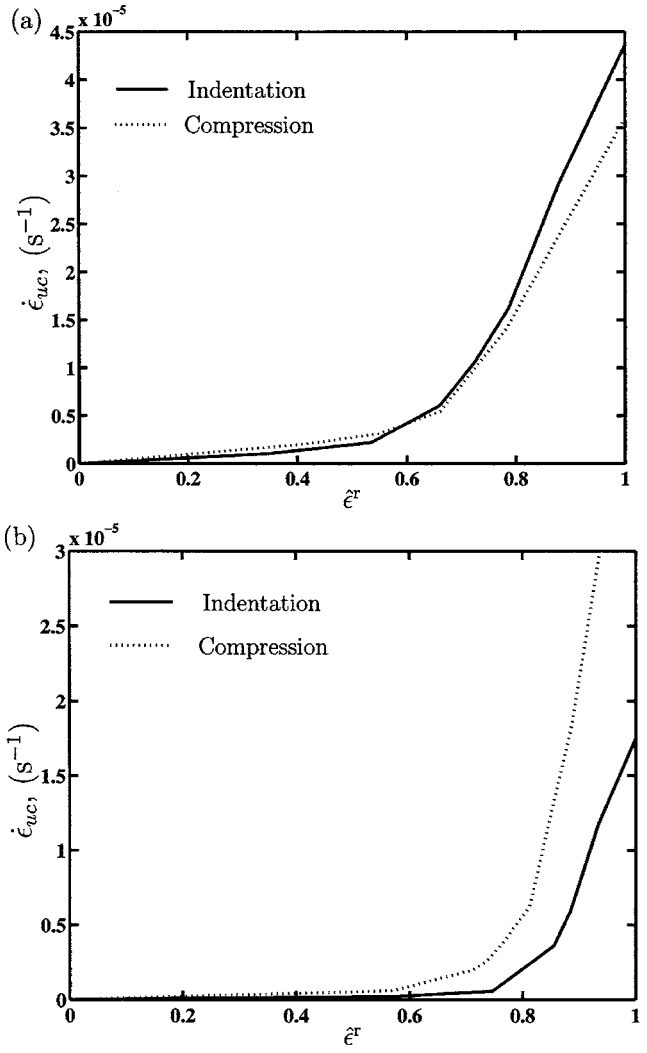

Fig. 10. Recovery calibration curves obtained from compression and indentation tests: (a) for Mixture A; (b) for Mixture B

deformation before reaching the corresponding steady-state strain and subsequent state of internal damage. On the other hand, the minimum values of $\dot{\epsilon}_{oc}$ are higher for the uniaxial compression results. This is consistent with the hydrostatic stress dependence of the mixtures, where an increase in confinement conditions generates a reduction on strain rate (stiffening effect). Fig. 13 shows the steady-state reference strain rate $\dot{\epsilon}_{oc}$ measured from triaxial compression and indentation experiments for both mixtures, with the indentation results depicted as horizontal lines as these tests implicitly account for the confinement conditions below the indenter. It is worth noting that the results cross at an *equivalent* stress ratio of $\eta \approx 0.4$ for both mixtures. It is expected that this *equivalent* stress ratio η is dependent on the dilation behavior of the mixtures, with higher values for lower dilation gradients and vice versa. For instance, researchers like Khanzada (2000) and Deshpande and Cebon (2004) studied numerically the stress field of a half-space of idealized asphalt mixtures loaded by a plane strain indenter, showing that the zone of maximum deformation is located at a semicircle of radius $R \approx a$, where the stress ratio $\eta \approx 0.6$, with a being the contact radius of the indenter. The relation between dilation behavior and *equivalent* stress ratio for indentation tests is a topic that merits further investigation.

A general reduction on the recovery strain rate $\dot{\epsilon}_{uc}$ on indenta-

J. Mater. Civ. Eng., 2007, 19(9): 753-761

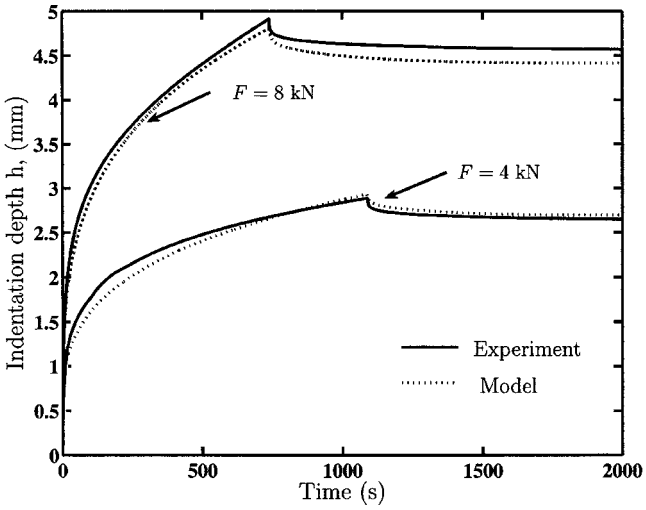

Fig. 11. Indentation creep recovery experimental measurements and model predictions at two selected values of total indentation depths h^T and indentation loads F at 15°C for Mixture A, with spherical indenter of diameter ϕ=200 mm

tion in comparison with compression results can also be observed in Fig. 10, similar to the results discussed previously.

Concluding Remarks

The model developed by Ossa et al. (2005) for the indentation behavior of bitumen has been successfully used to predict the indentation deformation response of asphalt mixtures. Monotonic and creep recovery indentation experiments were conducted at two specific temperatures on DBM mixtures composed of two different amounts of bitumen binder. The indentation model captures the experimentally observed indentation response accurately over a wide range of loading conditions. Moreover, the model is also successful in predicting the temperature dependence of the indentation response and the effect of the indenter diameter.

The volume fraction of bitumen plays an important role in the deformation behavior of the mixtures, increasing the deformation susceptibility with increasing volume, and enhancing the tertiary creep regime of behavior with a reduction of volume fraction of bitumen.

The parameters of the constitutive phenomenological model of Ossa et al. (2004a) were extracted from spherical indentation test results. A comparison with the model parameters obtained from uniaxial compression tests showed that indentation tests can be used in an easy and economical way to obtain the fundamental asphalt parameters. Further, parameters found from indentation tests implicitly account for the confining conditions generated by the aggregate particles below the indenter, which represent a valuable feature in the sense that no further triaxial tests are required to characterize the deformation behavior of the asphalt mixture.

The monotonic and recovery indentation behavior of asphalt investigated here is the primary problem for understanding the behavior of pavements under vehicle loads and is thus of intrinsic interest. The practicality and easy implementation of indentation tests allow for the determination of reliable material parameters in situ in a nondestructive way. Comparisons of indentation results

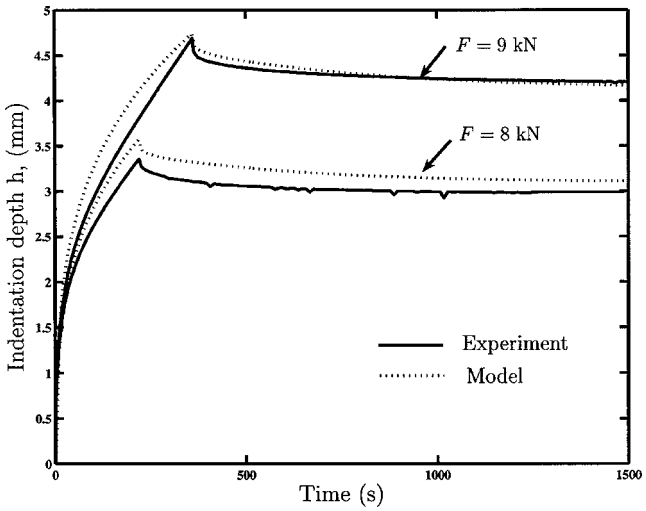

Fig. 12. Indentation creep recovery experimental measurements and model predictions at two selected values of total indentation depths h^T and indentation loads F at 20°C for Mixture B, with spherical indenter of diameter ϕ=200 mm

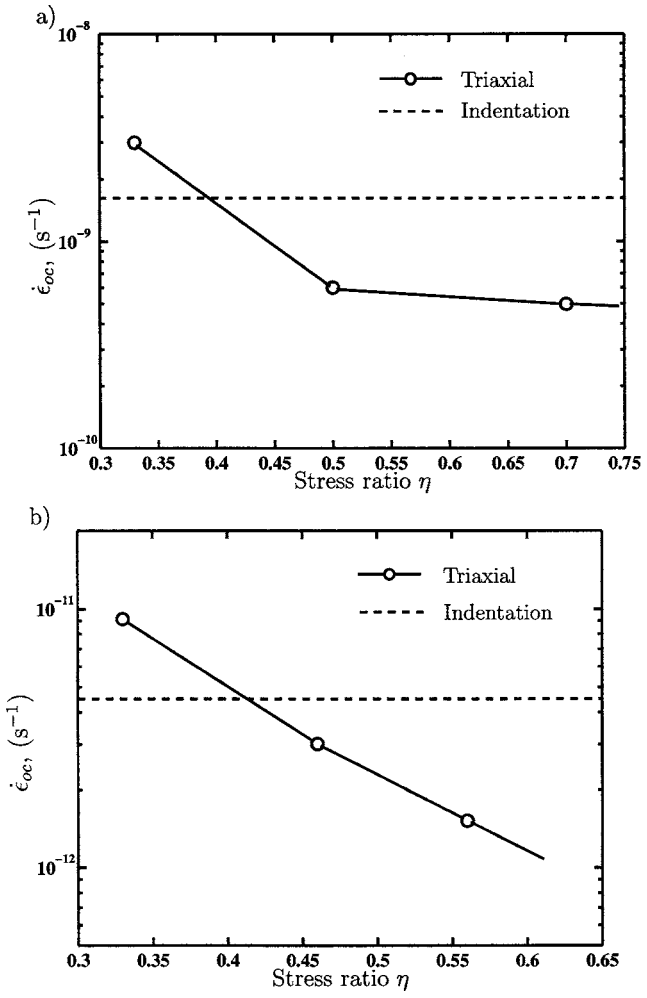

Fig. 13. Effect of stress ratio on steady-state constant $\dot{\epsilon}_{oc}$ on triaxial compression and indentation tests. Indentation results are depicted as dashed lines: (a) Mixture A; (b) Mixture B.

J. Mater. Civ. Eng., 2007, 19(9): 753-761

from laboratory specimens and in situ measurements is a topic which merits further investigation.

Acknowledgments

Support from the EPSRC Platform Grant awarded to the Nottingham Centre for Pavement Engineering (NCPE) is gratefully acknowledged.

References

Abbas, A. R., Papagiannakis, A. T., and Masad, E. A. (2004). "Linear and nonlinear viscoelastic analysis of the microstructure of asphalt concretes." *J. Mater. Civ. Eng.*, 16(2), 133–139.

Bower, A. F., Fleck, N. A., Needleman, A., and Ogbonna, N. (1993). "Indentation of a power law creeping solid." *Proc. R. Soc. London, Ser. A*, 441, 97–124.

British Standards Institution (BSI). (2003). "Part 1. Coated macadam for roads and other paved areas." *BS 4987-1*, London.

Chang, G. K., and Meegoda, N. J. (1993). "Simulation of the behavior of asphalt concrete using discrete element method." *Proc., 2nd Int. Conf. on Discrete Element Methods*, Massachusetts Institute of Technology Press, Cambridge, Mass., 437–448.

Cheung, C. Y., and Cebon, D. (1997). "Experimental study of pure bitumens in tension, compression, and shear." *J. Rheol.*, 41(1), 45–73.

Cheung, C. Y., Cocks, A. C. F., and Cebon, D. (1999). "Isolated contact model of an idealized asphalt mix." *Int. J. Mech. Sci.*, 41, 767–792.

Collop, A. C., and Khanzada, S. (2001). "Permanent deformation in idealised "sand asphalt" bituminous mixtures." *Int. Journal of Road Materials and Pavement Design*, 2(1), 7–28.

Collop, A. C., Scarpas, A., Kasbergen, C., and de Bondt, A. (2003). "Development and finite element implementation of stress-dependent elastoviscoplastic constitutive model with damage for asphalt." *Transportation Research Record. 1832*, Transportation Research Board, Washington, D.C., 96–104.

Cross, M. M. (1965). "Rheology of non-Newtonian fluids: A new flow equation for pseudoplastic systems." *J. Colloid Sci.*, 20, 417–437.

Deshpande, V. S., and Cebon, D. (1999). "Steady-state constitutive relationship for idealised asphalt mixes." *Mech. Mater.*, 31, 271–287.

Deshpande, V. S., and Cebon, D. (2000). "Uniaxial experiments on idealized asphalt mixes." *J. Mater. Civ. Eng.*, 12(3), 262–271.

Deshpande, V. S., and Cebon, D. (2004). "Micromechanical modeling of steady-state deformation in asphalt." *J. Mater. Civ. Eng.*, 16(2), 100–106.

Hill, R., Storakers, B., and Zdunek, A. B. (1989). "A theoretical study of the Brinell hardness test." *Proc. R. Soc. London, Ser. A*, 423, 301.

Huang, B., Mohammad, L. N., and Wathugala, G. W. (2002). "Development of a thermo-viscoplastic constitutive model for HMA mixtures." *J. Ass. Asphalt Paving Technol.*, 71, 594–618.

Huang, B., Mohammad, L. N., and Wathugala, G. W. (2004). "Application of a temperature dependent viscoplastic hierarchical single surface model for asphalt mixtures." *J. Mater. Civ. Eng.*, 16(2), 147–154.

Khanzada, S. (2000). "Permanent deformation in bituminous mixtures." Ph.D. thesis, Univ. of Nottingham, Nottingham, U.K.

Lee, H., and Kim, Y. R. (1998). "Viscoelastic constitutive model for asphalt concrete under cyclic loading." *J. Eng. Mech.*, 124(1), 32–40.

Long, F. M. (2001). "Permanent deformation of asphalt concrete pavements: A nonlinear viscoelastic approach to mix analyses and design." Ph.D. thesis, Univ. of California, Berkeley, Calif.

Lytton, R., Uzan, J., Fernando, E. G., Roque, R., Hiltunen, D., and Stoffels, S. M. (1993). "Development and validation of performance prediction models and specifications for asphalt binders and paving mixes." *Technical Rep. No. SHRP-A-357*, Strategic Highway Research Program, National Research Council, Washington, D.C.

Mulhearn, T. O., and Tabor, D. (1960). "Creep and hardness of metals: A physical study." *J. Inst. Met.*, 89, 7–12.

Nijboer, L. J. (1948). *Plasticity as a factor in the design of dense bituminous road carpets*, Elsevier, New York.

Ossa, E. A., Deshpande, V. S., and Cebon, D. (2004a). "Triaxial deformation behavior of bituminous mixes." *Technical Rep. No. CUED/C-MICROMECH/TR.96*.

Ossa, E. A., Deshpande, V. S., and Cebon, D. (2004b). "Uniaxial monotonic and cyclic behaviour of bituminous mixes." *Technical Rep. No. CUED/C-MICROMECH/TR.95*.

Ossa, E. A., Deshpande, V. S., and Cebon, D. (2005). "Spherical indentation behaviour of bitumen." *Acta Mater.*, 53, 3103–3113.

Ossa, E. A., Taherkhani, H., and Collop, A. C. (2006). "Compressive deformation behaviour of asphalt mixtures." *Journal of the Association of Asphalt Paving Technologists*, in press.

Ramsamooj, D. V., Ramadan, J., and Lin, G. S. (1998). "Model prediction of rutting in asphalt concrete." *J. Transp. Eng.*, 124(5), 448–456.

Schapery, R. A. (1984). "Correspondence principles and a generalised *j* integral for large deformation and fracture analysis of viscoelastic media." *Int. J. Fract.*, 25, 195–223.

Tabor, D. (1951). *Hardness of metals*, Clarendon, Oxford, U.K.

Zhao, Y., and Kim, Y. R. (2003). "Time-temperature superposition for asphalt mixtures with growing damage and permanent deformation in compression." *Transportation Research Record. 1832*, Transportation Research Board, Washington, D.C., 161–172.

Zhu, H., and Nodes, J. E. (2000). "Contact based analysis of asphalt pavement with the effect of aggregate angularity." *Mech. Mater.*, 32, 193–202.

J. Mater. Civ. Eng., 2007, 19(9): 753-761